There is plenty of asbestos at the bottom. The case of magnesite raw material contaminated with asbestos fibres

Original
There is plenty of asbestos at the bottom. The case of magnesite raw material contaminated with asbestos fibres / Gualtieri, Alessandro F; Malferrari, Daniele; Di Giuseppe, Dario; Scognamiglio, Valentina; Sala, Orietta; Gualtieri, Magdalena Lassinantti; Bersani, Danilo; Fornasini, Laura; Mugnaioli, Enrico. - In: SCIENCE OF THE TOTAL ENVIRONMENT. - ISSN 0048-9697. - 898:(2023), p. 166275. [10.1016/j.scitotenv.2023.166275]

Availability:
This version is available at: 11381/2967015 since: 2024-11-09T15:31:58Z

Publisher:
ELSEVIER

Published
DOI:10.1016/j.scitotenv.2023.166275

There is plenty of asbestos at the bottom. The case of magnesite raw material contaminated with asbestos fibres

Alessandro F. Gualtieri [ab], Daniele Malferrari [ab]*, Dario Di Giuseppe [a], Valentina Scognamiglio [a], Orietta Sala [a], Magdalena Lassinantti Gualtieri [c], Danilo Bersani [d], Laura Fornasini [d], Enrico Mugnaioli [e]

[a] *Department of Chemical and Geological Sciences, University of Modena and Reggio Emilia, Via G. Campi 103, 41125 Modena, Italy*
[b] Inter-Departmental Research and Innovation Centre on Construction and Environmental Services of the University of Modena and Reggio Emilia.
[c] *Department of Engineering "Enzo Ferrari", University of Modena and Reggio Emilia, Via Vivarelli 10, 41125 Modena, Italy*
[d] *Department of Mathematical, Physical and Computer Sciences, University of Parma, Parco Area delle Scienze 7/A 43124 Parma, Italy*
[e] *Department of Earth Sciences, University of Pisa, Via Santa Maria 53 56126 Pisa, Italy*

*Corresponding author, e-mail: daniele.malferrari@unimore.it

Science of the Total Environment
Submitted as ***Research paper***

ABSTRACT

Although all six asbestos minerals (the layer silicate chrysotile and five chain silicate species actinolite asbestos, amosite, anthophyllite asbestos, crocidolite and tremolite asbestos) are classified as carcinogenic, chrysotile is still mined and used in many countries worldwide. Other countries, like Italy, impose zero tolerance for all asbestos species but conflicting views repress the development of globally uniform treaties controlling international trade of asbestos-containing materials. Hence, countries with more severe legislations against the use of these hazardous materials lack of an international safety net against importation of non-compliant products. Raw materials that contain impurities of asbestos are challenging to regulate and are examples of short-circuits of the global trading system, resulting in embarrassing or disastrous situations. For the first time, we report the discovery of commercial magnesite raw materials contaminated with white asbestos (chrysotile). Magnesite is since decades used in countries like Italy for various industrial applications without being aware of the asbestos impurity. The fibres observed in all samples analysed have similar geometric parameters. The average length and width of the fibres are 6.0 and 0.11 μm, respectively, and the length value ranges from 0.62 to 56.7 μm, the width value from 0.01 to 0.06 μm. Quantitative analysis showed a chrysotile content around 0.01 wt.% not allowed by current regulations in Italy and many other state. More generally, our findings demonstrate that without shared policies aimed at regulating asbestos circulation on the global market, “asbestos-free” national policies will inevitably fail. We call for the revision of global directives on asbestos and implementation of standard analytical protocols for the assessment of asbestos in natural raw materials to never again have another magnesite case.

Keywords: Magnesite, Asbestos, Chrysotile, REACH, Rotterdam Convention, Electron microscopy.

1. Introduction

The term "asbestos" refers to the layer-silicate serpentine chrysotile (white asbestos) and five double-chain silicates (amphiboles): actinolite asbestos, amosite (cummingtonite-grunerite asbestos or brown asbestos), anthophyllite asbestos, crocidolite (riebeckite asbestos or blue asbestos) and tremolite asbestos (Case et al., 2011). The International Agency for Research on Cancer (IARC) classifies all the six asbestos species as "carcinogens for humans" (IARC, 2012). Nevertheless, in contrast to the firm position taken by the IARC, only the five amphibole asbestos species are globally banned, and many countries in the world still allow the use of chrysotile (Gualtieri, 2017).

International treaties and agreements aimed at regulating the trade of hazardous chemicals, including asbestos, have been stipulated. Due to disagreements over the use of chrysotile and asbestos fibres concentration limits a globally harmonized system is still lacking. Chrysotile remains a mineral of high socio-economic and industrial relevance as in many countries it still represents an important economic resource and its hazardousness is unrecognised or, at the very least, ignored. In addition, even in states where chrysotile has been banned, it is not easy to verify the coupling between government ratification of international conventions and successful enforcement of the ban (Joshi et al., 2006; Lin et al., 2019; Yoon et al., 2018), although feedbacks in many cases are from monitoring activities such as, for example, the implementation of policies for the search for asbestos substitutes, the enforcement of the national surveillance system of the incidence of mesothelioma, and the control over the removal of and its eventual transformation into End-of-Waste (Aryal and Morley, 2020; Chimed-Ochir et al., 2022; Marsili et al., 2017; Thives et al., 2022). In the face of these challenges, it is not surprising that the governing body of the Rotterdam Convention for Hazardous Chemicals has not yet managed to reach consensus for listing chrysotile in Annex III and thus compel producers to label chrysotile. This excellent tool for international trade control of dangerous chemicals is thus not available for chrysotile. It should be remarked that the inclusion of a chemical in the Rotterdam convention requires a unanimous vote of all the countries is needed, and only a handful of supplier or user countries block this.

In the European Union, the REACH compliance prohibits any intentional use of asbestos, but allows the presence of category 1A carcinogens, including asbestos fibres, as contaminant in concentrations <0.1wt.% without obligation of labelling. Both the Rotterdam Convention and the REACH compliance are in contrast with more severe domestic laws of some parties like Italy that applies "zero tolerance" (Dlg 257/92, 1992) for asbestos fibres; this means that the unauthorised supply, transport, use, including manufacture and handling of asbestos and any material containing asbestos, even in trace, is prohibited. Direct consequences of these legislative disagreements are that asbestos-containing materials (ACMs) may be unknowingly imported and used in countries that have banned all asbestos minerals. An even more complicated situation occurs when asbestos fibres are present as contaminants, perhaps even accidentally. This situation can occur in the exploitation of certain minerals that may contain impurities of naturally occurring asbestos (Gualtieri, 2020).

In this scenario, our research group has been working for several years in screening natural raw materials that potentially contains asbestos. Our work is strictly voluntary and motivated by the scientific conviction that only zero exposure of workers and the population is a guarantee for the elimination of asbestos-related health issues. The methodology of this environmental surveillance includes follow-up on reports and notifications from mining companies as well continuous survey of existing literature to uncover cases of raw materials contaminated with asbestos. Knowing the specific rock types and geologic conditions leading to the formation of asbestos, potentially contaminated mineral commodities can be identified. These include Mg-rich silicates like serpentinized olivine (Van Gossen et al., 2003), vermiculite (Addison, 1995; Larson et al., 2010) and many more although, over the years, special concerns have been raised about potential human exposure and risk from asbestos in consumer products containing cosmetic talcum powder, especially its use with infants (Burns et al., 2019; Emory et al., 2020; Finley et al., 2012; Fitzgerald et al., 2019; Gordon et al., 2014; Van Gossen et al., 2003).

Hitherto, our activity contributed to disclose the case of a Na-feldspar mined in Orani (Sardinia, Italy) contaminated with asbestos tremolite (Gualtieri et al., 2018) and the case of commercial chrysotile-rich brucite from China, where the use of chrysotile asbestos is allowed (Malferrari et al., 2021). In the case of the Orani feldspar, mined since 1970, the presence of asbestos was discovered in 2015 and the mining activity, in compliance with Italian law, was consequently stopped. Our work contributed to assess unequivocally the nature of the asbestos fibres as tremolite and to recommend a safe selective exploitation of the 'asbestos free' raw material (Gualtieri et al., 2018). In the case of the Chinese brucite (Malferrari et al., 2021), the Italian import flow was promptly halted and the processing sites were cleared, thus avoiding future legal and, most importantly, health complications.

Recently we discovered that magnesite ($MgCO_3$), a widespread industrial raw material, may be contaminated with asbestos. Magnesite is used in several industrial applications such as the production of insulating materials and coatings, as inorganic additive in ceramic inks, pigments and cements, for CO_2 sequestration and as MgO source. This mineral can be associated with serpentine (Tzamos et al., 2020) and eventually also with asbestos minerals when occurring in altered ophiolitic rocks (i.e., outcrops of basic/ultrabasic rocks representing relicts of oceanic crust or upper mantle). In fact, magnesite occurs in four types (Drnek et al., 2018; Pohl, 1990): (i) of sedimentary origin within ancient marine platform carbonate suites (Veitsch type); (ii) in ultramafic magmatic rocks (Kraubath type); (iii) in sedimentary fluviatile-limnic sediments overlying ultramafics (Bela Stena type); (iv) in metamorphosed ultramafics with high magnesite content (Greiner type). Sedimentary type (i) is assumed not to contain asbestos minerals while type (iii) and (iv) are of minor economic importance. On the contrary, the Kraubath type deposits are actively exploited and may contain asbestos minerals formed as a result of lithological transformation processes (see Supporting information for further details).

In this work, we report the results of a systematic investigation of samples of magnesite from Kraubath type deposits imported from Turkey (KT) and Greece (KG) for use in the Italian production of traditional ceramics. In the title of the paper, we have chosen to paraphrase the famous title of the lecture given by Richard Feynman at the annual American Physical Society meeting in 1959 to point out that asbestos is still among us and circulates in an insidious way. It is essential to bear in mind that magnesite, if uncontaminated, poses no risk. When, on the other hand, it is contaminated with asbestos even at low concentrations, in addition to being illegal in many states, it poses a serious health risk, as shown by the numerous studies on chrysotile toxicity (see Gualtieri, 2023 for a recent review).

2. Materials and Methods

2.1. Samples

Representative samples of magnesite from Kraubath type deposits imported from Turkey (KT) and Greece (KG) and used in Italian manufacture sites of traditional ceramics have been investigated. The geological description of the two areas is reported in the Supporting Information. Both fine powders (KT1 and KG1) and lumps (KT2 and KG2) from the same deposits have been analysed. The samples were collected from distributers as well as from industrial end-users. A granulated commercial product of sedimentary Veitsch type from Austria, from now on called VA, was also included in the investigation together with various brands of commercial fine magnesite powders sold by Italian sporting goods retailers as anti-slip agent for various sports activities such as climbing. Among these powders, a commercial hydro-magnesite was also included.

2.2 X-ray powder diffraction

The mineralogical characterization of the magnesite samples was performed by X-Ray Powder Diffraction (XRPD) using an X'Pert-PRO PANanalytical θ/θ diffractometer (CuK_α radiation, 40kV and 40 mA), equipped with a Real Time Multiple Strip detector and Ni filter on the secondary beam. Data were collected from 3 to 80 °2θ, with a virtual scan time of 5s/step and step scan of 0.0167 °2θ. The XRPD spectra were preliminary analysed using the X-Pert High Score Plus software. A 1/2° divergence slit and a 0.2 mm receiving slit were used. The quantitative mineralogical analysis was performed with the Rietveld method (Rietveld, 1969) using the General Structure Analysis System (GSAS) software package (Larson and Von Dreele, 1994) with the graphical interface EXPGUI (Toby, 2001) and following the protocol reported in Gualtieri et al. (2019). More in detail, XRPD patters background was modelled using a Chebyshev polynomial of the first kind, peak shapes were modelled using the Thompson–Cox–Hastings pseudo-Voigt function, and March-Dollase function was chosen as intensity correction factor for preferred orientations and applied to the reflections (104) of magnetite and (001) of serpentine. The starting structural models used for the refinement are from Graf (1961) for magnesite, Gualtieri (2000) for quartz, Steinfink and Sans (1959) for dolomite, Ondrus et al. (2003) for calcite, Lister and Bailey (1967) for chlorite and Manceau et al. (1998) for smectite. Lizardite from Mellini (1982) was chosen as the starting structural model for quantitative estimation of serpentine.

2.3 Thermal analyses and evolved gasses mass spectrometry

Thermogravimetric (TGA) and thermo-differential (DTA) analyses were performed with a Seiko SSC 5200 thermal analyser coupled with quadrupole mass spectrometer (ESS, GeneSys Quadstar 422) to detect gases released during thermal reactions (MSEGA). Gas sampling was done using a silicon capillary pre-heated to avoid gas condensation. Experimental conditions were: heating rate: 20 °C/min; heating range: 25-1000 °C; TGA and DTA data measurement: every 0.5 s; DTA reference: α-alumina powder; purging gas: ultrapure helium with a flow rate of 100 μL/min. Mass analyses were performed in multiple ion detection mode by measuring m/z ratios (i.e., the dimensionless ratio of the mass number m to the z-charge of an ion) 18, 30, 44, 64 to detect the emission of H_2O, NO, CO_2, and SO_2, respectively using a secondary electron multiplier (SEM) detector set at 900 V with 1 s integration time on each measured mass.

2.4 Optical microscopy analyses

Preliminary observation of the raw sample (KT2) with A Meiji Techno stereomicroscope (50x) showed that the green veins are characterised by an intergrowth of green plate-like mineral grains with bundles of white mineral fibres with a length between 0.5-0.7 mm. Fibres were picked up using tweezers and subsequently characterised with Phase Contrast Optical Microscope (PCOM). PCOM analyses were conducted following the methodology proposed by Di Giuseppe et al. (2021) for the identification of chrysotile. Analyses were carried out using an Olympus BX51 phase-contrast microscope and Cargille Refractive Index (RI) Liquid n = 1.550. Two drops of refractive index medium were placed on a pre-cleaned glass slide (76×26 mm). Few representative fibres or bundles were placed on the slide and covered with a cover slip. PCOM observations were made in both phase contrast and dark field mode. The PCOM technique was not applied to powder magnesite samples due to the small size of the fibres in these samples.

2.5 Electron microscopy

The morphological observation of the samples was carried out by a Scanning Electron Microscope (SEM) using JSM-6010PLUS/LA (JEOL, Hillsboro, OR, USA) equipped with an Energy Dispersive X-ray (EDX) microanalysis system (Oxford INCA-350) and Field Emission Gun Scanning Electron Microscope (FEG-SEM) FEI Nova NanoSEM 450 FEG-SEM. According with the Italian Minister Decree 06.09.94 (DM September 06, 1994) the procedure for quantitative SEM analysis was performed as follows: an amount of 5 mg of the sample was suspended in 200 ml of deionized water with 0.1 vol.% surfactant additive (dioctylsodium sulfoccinate, $C_{20}H_{37}NaO_7S$, CAS no. 577-11-7), and ultrasonicated for 10 min to promote particle separation. A volume of 6 ml of this suspension was collected at different levels in a becker and placed in a filtration system, allowing random deposition of the particles on polycarbonate filters (20 mm^2 surface, 0.45 μm porosity). Then the filter was dried at 55 °C and weighed. The final weight of the material deposited on the filter was 0.1 mg. The filter was mounted on an aluminium stub and coated with gold using a Carbon Coater-Balzers CED-010 (10 nm thick). The SEM images were obtained by secondary electron imaging covering 1 mm^2 of surface at 4000× magnification (130 analysis fields).

The powder samples KT1 and KG1 were investigated as received while small fragments of the raw KT2 and KG2 samples were gently ground in agate mortar to obtain a fine powder. A small amount of sample was suspended with 1 mL of ethanol in a test tube, sonicated for 1 min (using a low power sonic bath) and left to set for 5 min. A drop of the suspension was then transferred and dried onto a 300-mesh carbon copper TEM grid.

Preliminary TEM investigations focused on the microstructure of the mineral fibres in the samples were carried out at the CIGS-UNIMORE laboratories by using a Talos F200S G2 microscope, equipped with S-FEG Schottky field emitter operating at 200 kV and two large-area EDX spectrometers with Silicon Drift Detectors (SDD).

High resolution transmission electron microscopy (HRTEM), energy-dispersive X-ray spectroscopy (EDS) and three-dimensional electron diffraction (3DED) were performed with a JEOL JEM-F2000 Multi-purpose, working at 200 kV and equipped with Schottky-FEG source and SDD EDS detector. 3DED data were analysed and visualized by ADT3D software (Gemmi et al., 2019; Kolb et al., 2011).

2.6 Micro-Raman spectroscopy

The Raman spectra were collected on the magnesite powders (KT1 and KG1) and on a fragment (KT2) with a HORIBA Jobin Yvon LabRam confocal micro-spectrometer (300 mm focal length), using a He-Ne 632.8 nm and a frequency doubled Nd:YAG 473.1 nm laser lines as excitation sources, with an integrated Olympus BX40 microscope with 4×, 10×, 50× ULWD and 100× objectives, a 1800 grooves/mm grating, a XY motorized stage and a Peltier cooled silicon CCD. The spectral resolution is ~2 cm^{-1} with the 632.8 nm line and ~4 cm^{-1} with the 473.1 nm line. The system was calibrated by using the 520.6 cm^{-1} Raman peak of silicon in the low-wavenumber spectral region (100-1200 cm^{-1}) and the emission lines of a gas lamp in the high-wavenumber spectral region (3000-4000 cm^{-1}). The spectra have been recorded with typical exposures of 60 s repeated at least 4 times. Data analysis has been performed by LabSpec 5 built-in software. Fit with bands deconvolution has been carried out with Gauss-Lorentzian functions.

3. Results

The XRPD data on the magnesite samples show a number of secondary phases (Table 1). The mineralogical composition (wt%) of samples KT1 and KG1, performed using Rietveld's quantitative phase analysis (Fig. 1 and Table 2), revealed magnesite, quartz, serpentine and dolomite in sample KT1, while talc, calcite, smectite and chlorite were also identified in sample KG1.

In addition to the magnesite decarbonation, the TGA/DTA-MSEGA analyses highlight, in samples polluted with chrysotile, the typical dehydroxylation reaction of the octahedral sheet of chrysotile followed by an exothermic event indicating its recrystallization in forsterite (Bloise et al., 2016; Cattaneo et al., 2003; Khorami et al., 1984). For both KT1 and KG1, the TGA curves and their first derivative (DTG) show one principal (1) and one minor (2) thermal event, which are both attributed to multiple fully or partially overlapping thermal reactions. An additional thermal event (3) is evidenced by the DTA curve, but only for KT1.

In KT1 (Fig. 2a) reaction (1) occurs in the temperature range 445-640 °C (maximum reaction rate at 599 °C) and results in a mass loss of 42.1 wt%. Reaction (2), which occurs between 650 and 735 °C is less evident and produced a mass loss of 1.0 wt%. The DTA curve (Fig. 2b), in addition to the endothermic signals related to reactions (1) and (2), also highlights a weak exothermic reaction (3) with a maximum at about 830 °C. The release of CO_2 (m/z=44, Fig. 2c) associated with reaction (1) proves that this thermal event occurs following the decarbonation of magnesite (mainly) and of dolomite (first step). On the other hand, reaction (2) involves the simultaneous release of H_2O (m/z=18, Fig. 2c) and CO_2 that could be respectively related to the dehydroxylation of the serpentine and to the second step of dolomite decarbonation according to the well-known thermal decomposition mechanism (Bloise et al., 2016):

$$CaMg(CO_3)_2 \rightarrow MgO + CaCO_3 + CO_2 \rightarrow MgO + CaO + CO_2$$

where the first step is not distinguishable as completely overlapping with reaction (1). Reaction (3) is due to the recrystallization of the serpentine in forsterite occurring after dehydroxylation (Bloise et al., 2016; Cattaneo et al., 2003; Khorami et al., 1984). Below 250 °C, it is also possible to observe weak reactions, more evident in the magnification of Fig. 2a and in MSEGA curve m/z=18 (Fig. 2c), related to the removal of more or less strongly bound water molecules.

The thermal behavior of sample KG1 nearly parallels that of KT1 and is described in the Supporting Information.

Macroscopic fibre bundles were discovered in the raw rock samples. For example, the macroscopic observation of the raw KT2 sample composed of centimetric rock fragments (Fig. 3a) shows green lamellar mineral phases and white mineral fibres (L= 0.5–0.7 mm). The latter were selected and observed with PCOM and revealed beautiful bundles of chrysotile fibres (Fig. 3b). The PCOM technique allowed to easily identify the nature of the fibres in KT2. In fact, fibres treated with RI=1.550 liquid displayed the characteristic dispersion colours of chrysotile (Di Giuseppe et al., 2021). Observed in phase contrast mode, fibres colour was light blue with an orange halo when the fibre axis was perpendicular to the polariser, and dark blue with an orange halo when the fibre axis was parallel to the polariser (Fig. 3b).

The SEM images of raw and powder magnesite samples from Turkey (KT1, KT2) and Greece (KG1, KG2) show a matrix of massive magnesite particles with several flexible bundles of chrysotile fibres (Fig. 4a-d) whose nature has been confirmed by the EDX analyses (Fig. 4 e,f). A series of representative SEM images were analysed using *ImageJ* software, which provides accurate measurements of the length and width of the chrysotile fibre. The fibres observed in the Turkish (KT1) and Greek (KG1) powders samples have the same geometrical parameters. The average fibre length and width are 6.0 and 0.11 µm respectively. The length value ranges from 0.62 to 56.7 µm, the width from 0.01 to 0.06 µm.

Most of the fibres display the so-called “Stanton size”: based on *in vivo* animal studies, asbestos fibres longer than 8 µm and thinner than 0.25 µm are strongly carcinogenic and induce malignant pleural mesothelioma (Stanton et al., 1981; Stanton and Wrench, 1972). The quantitative SEM analysis carried out according to the Italian Ministry of Health regulations and technical methodologies (DM September 06, 1994) highlighted a chrysotile content of 0.012 wt.% for KT1 (0.012 wt.% for KT2 and 0.010 wt.% for the KG samples).

TEM observations confirm that chrysotile is the fibrous phase present in the investigated Turkish and Greek magnesite samples. In particular, sample KT2 contains fibres long up to few microns and thick up to 80 nm (Fig. 5a). A closer look reveals that these fibres have a nanotube structure, with internal channels that may be more or less visible and large up to 30-40 nm (Fig. 5b). More massive fragments are also present in the KT2 sample, although with a significantly lower incidence. EDS measurements show that both fibres and massive fragments have a comparable composition, consistent with serpentine minerals (Fig. 5c). 3DED analysis confirms that the fibres are chrysotile; the reconstructed diffraction volume shows typical crowns of diffuse scattering produced by the bending of the serpentine layers (Fig. 5d). 3DED also reveals that massive fragments consist of lizardite or polygonal serpentine; the latter is easily recognizable due to the circular crowns of reflections arranged according to a pseudo five-fold symmetry (Fig. 5e) (Baronnet et al., 1994). All the other samples consist mostly of magnesite crystals of different size. Elongated tubular fibres are also spotted very frequently. Some fibres display a habit similar to the chrysotile detected in sample KT2, but the most common form consists of bent hair-like fibres typically arranged in crowded bundles (see for example the chrysotile fibres in sample KG2 reported in Fig. 5f).

The Micro-Raman data confirm the results obtained with the other experimental techniques. The signal of chrysotile was detected in both Turkish and Greek samples. In the Turkish powder KT1, lizardite was also observed, and its signal sometimes appears in conjunction with that of chrysotile. In the low-wavenumber spectral range, the Raman signals related to the lattice vibrational modes and the internal vibration of the SiO_4 tetrahedra of a serpentine phase were observed in KT1 (at 229, 385, 619, 690 cm^{-1}) and in KG1 (at 392, 689 cm^{-1}) (Fig. 6a). The contribution of magnesite from the surrounding crystals was also detected (at 211, 329, 738, 1094 cm^{-1}) (Fig. 6a). The univocal identification of chrysotile in the powders was confirmed by its peculiar Raman bands of the OH stretching vibrations (Fornasini et al., 2022), between 3500-3800 cm^{-1}, with an intense peak at ~3695 cm^{-1} and a weak contribution at ~3647 cm^{-1} (Fig. 6b). Typically, the most intense peak of chrysotile is also characterized by a shoulder at ~3680 cm^{-1}, which is markedly pronounced in KT1. A possible contribution due to lizardite, in addition to chrysotile, may explain this curve shape, since its most intense OH stretching signal occurs at 3683 cm^{-1} (Auzende et al., 2004; Petriglieri et al., 2015). The presence of chrysotile in KT1 was supported by the analysis on the raw fragment (KT2), whose Raman spectrum corresponds to that of chrysotile (characteristic peaks occurring at 233, 391, 691 and 1104 cm^{-1} in the low-wavenumber range and at 3697 with a shoulder at ~3687 cm^{-1} in the OH stretching region).

4. Discussion

Our systematic investigation clearly shows that a small amount of chrysotile is present as the only asbestos phase in the Kraubath type industrial minerals from Greece and Turkey. The Austrian granulate of sedimentary Veitsch type (VA) as well the powders sold at retail as anti-slip agent do not contain asbestos at all. We rule out the possibility of contamination during materials processing of the industrial minerals as chrysotile fibres were found in both the powders and the raw fragmented rocks. Only the use of a suite of different experimental techniques made it possible to assess indisputably that chrysotile is present in these magnesite products. In this context, XRPD and TGA/DTA are inconclusive methods while micro-Raman and electron microscopy techniques are decisive for revealing the true crystal-chemical nature of the fibres. Fine powders are particularly challenging and high-resolution electron microscopy analyses of carefully prepared specimens are indispensable for revealing the presence of fibre bundles. Hence, even actors in the supply chain that have actively searched for asbestos contaminants may have failed due to inadequate analysis methods. Together with the lack of adequate and shared analytical protocols, this could be a reason why chrysotile was not revealed before by the magnesite producers.

In Italy, this magnesite product has been used as raw material in the traditional ceramics industry for decades without being aware of the asbestos contaminant. Our discovery reveals major flaws in the global network and a number of violations and conflicts. Regarding the violations, asbestos contaminated magnesite should be considered as illicit in countries like Italy, Germany and France where the marketing of all ACMs, with a few exceptions, where banned during the 90s (Décret 96-1133, 1996; dlg 257/92, 1992; Gesetz 162, 1993). This applies also to industrial minerals where asbestos has not been intentionally added even in very low concentration. There is also a violation of the 2009 European directive (EC 2009/148, 2009) on the protection of workers from the risks related to exposure to asbestos at work as "*Even though it has not yet been possible to identify the exposure threshold below which asbestos does not involve a cancer risk, occupational exposure to workers to asbestos should be reduced to a minimum*." Another violation regards the fact that, according to the 2006 EU Regulation (EC 2006/1907, 2006), all articles containing asbestos must bear the "asbestos" label. Unfortunately, a number of conflicts and discrepancies make the actual situation chaotic. The 2006 EU Regulation specifically prohibits the placing on the market of articles and mixtures containing asbestos fibres "*added intentionally*". Because chrysotile is not added intentionally to magnesite but is a natural contaminant, is this "article" out of the 2006 EU Regulation? The same Regulation admits a content of carcinogens, including asbestos, of 0.1 wt%. In this case, the Turkish magnesite powder (KT1) for example, with a chrysotile content of 0.012 wt.%, would be legal in the EU.

Regarding importation from extra-EU countries, the Rotterdam convention is a precious tool for the adhering parties (including EU countries) in avoiding accidental importation of domestically forbidden substances. In fact, the Rotterdam Convention deals with "*substances whether by itself or in a mixture …*" (Article 1) with no specification of the quantity except for a generic statement on "*…chemicals in quantities not likely to affect human health…*" (Article 3); the latter, however, is not the case though because it is well known that there is no evidence for a threshold or a "safe" level of asbestos exposure (see for example, Lemen and Landrigan, 2017). Each party is obliged to guarantee that exporters within its jurisdiction do not ship listed chemical to other parties that disapproves importation of them. This multilateral treaty regulates the international trade of hazardous chemicals, listed in Annex III to the convention. Whereas amphibole asbestos species are listed, chrysotile is still only recommended for listing by the Chemical Review Committee. The outcome is that legal responsibilities shift from exporters to importers, with an obvious increased risk of finding non-compliant products on the European market. Hence, in countries like Italy, asbestos contaminated magnesite is automatically out of law only when it is already present in its territory.

This chaos in the global market of ACMs has negative consequences for countries that wish to protect people from any exposure to asbestos fibres. For example, workers handling industrial raw materials containing unknown asbestos contaminants do not make adequate use of protective measures and the exposure risk increases (Burdett and Bard, 2007; Douglas and Van den Borre, 2019). The Individual companies can suffer from severe economic losses and legal issues if the presence of ACMs is discovered by the local environmental/health authorities. The site can be impounded by a state's attorney with the suspension of the working activity and access prohibited until the end of the legal action. This was the case with the Italian feldspar mine contaminated with tremolite asbestos (Gualtieri et al., 2018).

It is sad to acknowledge that countries (like Italy) hardly targeting to turn “asbestos-free” (Terracini, 2019) or at least “asbestos-safe” see their efforts thwarted by the income of new contaminated materials on their territory without their knowledge.

5. Conclusions

The global use of asbestos is decreasing worldwide (Frank and Joshi, 2014) but is still not zero. Naturally occurring asbestos (Gualtieri, 2020) is another threat to the public health that transforms from local to geographically widespread when the fibres are present as impurity in industrial minerals that may freely circulate among states seriously impacting the total environment. The magnesite case reported here is a perfect example of this type of situation and proves that there is still plenty of asbestos at the bottom. Our research group will continue the screening of commercial raw materials in search of asbestos for predictive purposes. We have to avoid *ex post* discovering of the exposure of the population or workers to some mineral source through the observation of malignant mesothelioma morbidity peaks as was the case in the past for fluoro-edenite in Biancavilla (Italy) (Comba et al., 2003) or fibrous erionite in Cappadocia (Turkey) (Baris et al., 1987).

In concrete terms, we believe that without a global ban of asbestos (Douglas and Van den Borre, 2019), which appears to be utopic at the moment, only shared harmonized policies aimed at regulating asbestos mining and circulation adopted by all the countries that have banned asbestos and that aspire to become asbestos-free can drive us to see the light at the end of the tunnel. We call for a harmonized standard analytical protocol: when imported, each raw material and especially those of asbestos-compatible origin, must be accompanied by a certification of absence of asbestos phases, assessed by a suite of analytical determination also including high-resolution SEM or TEM, that producers (the mining companies) deliver. The importing company/national distributors can randomly cross-check the reliability of the certificates by validated specialized labs using the analytical methodologies mentioned above. Following the case of the talc mining industry (Schlossman, 2009) and the example of New Caledonia where the exploitation of serpentine rocks contaminated by asbestos is strictly regulated (Worliczek, 2017), mining activity in asbestos-rich or supposedly asbestos-rich national deposits should be always carried out under severe monitoring and differential processing to avoid exploitation of asbestos-rich levels. As for the case above, the domestic distribution of the raw materials delivered to the production sites must be accompanied by a certification of absence of asbestos phases.

The conflict between the European REACH compliance (EC 2006/1907, 2006) that admits a content of carcinogens, including asbestos, of 0.1 wt% in circulating raw materials, and the national laws must be resolved by making an exception for asbestos in the list of REACH carcinogens so that, compatible with the SEM experimental detection limits, the raw materials should not contain asbestos phases.

Finally, at a global level, we call for the inclusion of chrysotile in the list of Rotterdam convention of Hazardous Chemicals under the Rotterdam Convention to be labelled for import/export operations.

CRediT authorship contribution statement

Alessandro F. Gualtieri: Supervision, Project administration, Conceptualization, Resources, Formal analysis, Methodology, Validation, Writing the original draft, Writing, review and editing, Funding acquisition. Daniele Malferrari: Supervision, Methodology, Validation, Writing, review and editing, Funding acquisition. Dario Di Giuseppe: Investigation, review and editing. Valentina Scognamiglio: Investigation, review and editing. Orietta Sala: Investigation, review and editing. Magdalena Lassinantti Gualtieri: Conceptualization, Writing the original draft, Writing, review and editing. Danilo Bersani: Investigation, Writing – review and editing.

Laura Fornasini: Investigation, Writing – review and editing. Enrico Mugnaioli: Investigation, Writing – review and editing.

Acknowledgments

The work is supported by the PRIN project fund "Fibres: a multidisciplinary mineralogical, crystal-chemical and biological project to amend the paradigm of toxicity and cancerogenicity of mineral fibres" (PRIN: Progetti di Ricerca di Rilevante Interesse Nazionale—Bando 2017—Prot. 20173X8WA4). Authors thanks the Center for Instrument Sharing of the University of Pisa (CISUP), Italy, for the TEM measurements.

Data availability

Data will be made available on request.

Declaration of competing interest

The authors declare that they have no known competing financial interests or personal relationships that could have appeared to influence the work reported in this paper.

References

Addison, J., 1995. Vermiculite: a review of the mineralogy and health effects of vermiculite exploitation. Regul. Toxicol. Pharmacol. RTP 21, 397–405. https://doi.org/10.1006/rtph.1995.1054

Aryal, A., Morley, C., 2020. Call for a global ban policy on and scientific management of asbestos to eliminate asbestos-related diseases. J. Public Health Policy 41, 279–285. https://doi.org/10.1057/s41271-020-00223-4

Auzende, A.-L., Daniel, I., Reynard, B., Lemaire, C., Guyot, F., 2004. High-pressure behaviour of serpentine minerals: a Raman spectroscopic study. Phys. Chem. Miner. 31, 269–277. https://doi.org/10.1007/s00269-004-0384-0

Baris, I., Simonato, L., Artvinli, M., Pooley, F., Saracci, R., Skidmore, J., Wagner, C., 1987. Epidemiological and environmental evidence of the health effects of exposure to erionite fibres: a four-year study in the Cappadocian region of Turkey. Int. J. Cancer 39, 10–17. https://doi.org/10.1002/ijc.2910390104

Baronnet, A., Mellini, M., Devouard, B., 1994. Sectors in polygonal serpentine. A model based on dislocations. Phys. Chem. Miner. 21. https://doi.org/10.1007/BF00202098

Bloise, A., Catalano, M., Barrese, E., Gualtieri, A.F., Bursi Gandolfi, N., Capella, S., Belluso, E., 2016. TG/DSC study of the thermal behaviour of hazardous mineral fibres. J. Therm. Anal. Calorim. 123, 2225–2239. https://doi.org/10.1007/s10973-015-4939-8

Burdett, G., Bard, D., 2007. Exposure of UK Industrial Plumbers to Asbestos, Part I: Monitoring of Exposure Using Personal Passive Samplers. Ann. Occup. Hyg. 51, 121–130. https://doi.org/10.1093/annhyg/mel078

Burns, A.M., Barlow, C.A., Banducci, A.M., Unice, K.M., Sahmel, J., 2019. Potential Airborne Asbestos Exposure and Risk Associated with the Historical Use of Cosmetic Talcum Powder Products. Risk Anal. 39, 2272–2294. https://doi.org/10.1111/risa.13312

Case, B.W., Abraham, J.L., Meeker, G., Pooley, F.D., Pinkerton, K.E., 2011. Applying Definitions of “Asbestos” to Environmental and “Low-Dose” Exposure Levels and Health Effects, Particularly Malignant Mesothelioma. J. Toxicol. Environ. Health B Crit. Rev. 14, 3–39. https://doi.org/10.1080/10937404.2011.556045

Cattaneo, A., Gualtieri, A.F., Artioli, G., 2003. Kinetic study of the dehydroxylation of chrysotile asbestos with temperature by in situ XRPD. Phys. Chem. Miner. 30, 177–183. https://doi.org/10.1007/s00269-003-0298-2

Chimed-Ochir, O., Rath, E.M., Kubo, T., Yumiya, Y., Lin, R.-T., Furuya, S., Brislane, K., Klebe, S., Nowak, A.K., Kang, S.-K., Takahashi, K., 2022. Must countries shoulder the burden of mesothelioma to ban asbestos? A global assessment. BMJ Glob. Health 7, e010553. https://doi.org/10.1136/bmjgh-2022-010553

Comba, P., Gianfagna, A., Paoletti, L., 2003. Pleural mesothelioma cases in Biancavilla are related to a new fluoro-edenite fibrous amphibole. Arch. Environ. Health 58, 229–232. https://doi.org/10.3200/AEOH.58.4.229-232

Décret 96-1133, 1996. Décret n°96-1133 du 24 décembre 1996 relatif à l’interdiction de l’amiante, pris en application du code du travail et du code de la consommation, 96-1133.

Di Giuseppe, D.D., Zoboli, A., Nodari, L., Pasquali, L., Sala, O., Ballirano, P., Malferrari, D., Raneri, S., Hanuskova, M., Gualtieri, A.F., 2021. Characterization and assessment of the potential toxicity/pathogenicity of Russian commercial chrysotile. Am. Mineral. 106, 1606–1621. https://doi.org/10.2138/am-2021-7710

Dlg 257/92, 1992. Italian Law n. 257/92 (Legge 27 marzo 1992, n. 257 - Norme relative alla cessazione dell’impiego dell’amianto). In Suppl. Ord. alla Gazzetta Ufficiale 87 del 13 aprile 1992.

DM September 06, 1994. Italian Ministry of Health - Gazzetta Ufficiale della Repubblica Italiana - Normative e metodologie tecniche di applicazione dell’art.6, comma 3, e dell’art.12, comma 2, della legge 27 marzo 1992, n.257, relativa alla cessazione dell’impiego dell’amianto.

Douglas, T., Van den Borre, L., 2019. Asbestos neglect: Why asbestos exposure deserves greater policy attention. Health Policy 123, 516–519. https://doi.org/10.1016/j.healthpol.2019.02.001

Drnek, T., Moraes, M., Neto, P., 2018. Overview of magnesite. J. Refract. Innov. RHIM Bull. 1, 14–22.

EC 2006/1907, 2006. Regulation (EC) N. 1907/2006 of the European Parliament and of the Council of 18 December 2006 concerning the Registration, Evaluation, Authorisation and Restriction of Chemicals (REACH), establishing a European Chemicals Agency, amending Directive 1999/45/EC and repealing Council Regulation (EEC) N. 793/93 and Commission Regulation (EC) N. 1488/94 as well as Council Directive 76/769/EEC and Commission Directives 91/155/EEC, 93/67/EEC, 93/105/EC and 2000/21/EC.

EC 2009/148, 2009. Directive 2009/148/EC of the European Parliament and of the Council of 30 November 2009 on the protection of workers from the risks related to exposure to asbestos at work.

Emory, T.S., Maddox, J.C., Kradin, R.L., 2020. Malignant mesothelioma following repeated exposures to cosmetic talc: A case series of 75 patients. Am. J. Ind. Med. 63, 484–489. https://doi.org/10.1002/ajim.23106

Finley, B.L., Pierce, J.S., Phelka, A.D., Adams, R.E., Paustenbach, D.J., Thuett, K.A., Barlow, C.A., 2012. Evaluation of tremolite asbestos exposures associated with the use of commercial products. Crit. Rev. Toxicol. 42, 119–146. https://doi.org/10.3109/10408444.2011.636028

Fitzgerald, S., Harty, E., Joshi, T.K., Frank, A.L., 2019. Asbestos in commercial indian talc. Am. J. Ind. Med. 62, 385–392. https://doi.org/10.1002/ajim.22969

Fornasini, L., Raneri, S., Bersani, D., Mantovani, L., Scognamiglio, V., Di Giuseppe, D., Gualtieri, A.F., 2022. Identification of iron compounds in chrysotile from the Balangero mine (Turin, Italy) by micro-Raman spectroscopy. J. Raman Spectrosc. 53, 1931–1941. https://doi.org/10.1002/jrs.6434

Frank, A.L., Joshi, T.K., 2014. The global spread of asbestos. Ann. Glob. Health 80, 257–262. https://doi.org/10.1016/j.aogh.2014.09.016

Gemmi, M., Mugnaioli, E., Gorelik, T.E., Kolb, U., Palatinus, L., Boullay, P., Hovmöller, S., Abrahams, J.P., 2019. 3D Electron Diffraction: The Nanocrystallography Revolution. ACS Cent. Sci. 5, 1315–1329. https://doi.org/10.1021/acscentsci.9b00394

Gesetz 162, 1993. Gesetz zu dem Übereinkommen Nr. 162 der Internationalen Arbeitsorganisation vom 24. Juni 1986 über Sicherheit bei der Verwendung von Asbest.

Gordon, R.E., Fitzgerald, S., Millette, J., 2014. Asbestos in commercial cosmetic talcum powder as a cause of mesothelioma in women. Int. J. Occup. Environ. Health 20, 318–332. https://doi.org/10.1179/2049396714Y.0000000081

Graf, D., 1961. Crystallographic tables for the rhombohedral carbonates. American Mineralogist: Journal of Earth and Planetary Materials. J. Earth Planet. Mater. 46, 1283–1316.

Gualtieri, A.F., 2023. Journey to the centre of the lung. The perspective of a mineralogist on the carcinogenic effects of mineral fibres in the lungs. J. Hazard. Mater. 442, 130077. https://doi.org/10.1016/j.jhazmat.2022.130077

Gualtieri, A.F., 2020. Naturally Occurring Asbestos: A Global Health Concern? State of the Art and Open Issues. Environ. Eng. Geosci. 26, 3–8. https://doi.org/10.2113/EEG-2271

Gualtieri, A.F. (Ed.), 2017. Mineral fibres: Crystal chemistry, chemical-physical properties, biological interaction and toxicity, 1st ed. Mineralogical Society of Great Britain & Ireland. https://doi.org/10.1180/EMU-notes.18

Gualtieri, A.F., 2000. Accuracy of XRPD QPA using the combined Rietveld–RIR method. J. Appl. Crystallogr. 33, 267–278. https://doi.org/10.1107/S002188989901643X

Gualtieri, A.F., Gandolfi, N.B., Pollastri, S., Rinaldi, R., Sala, O., Martinelli, G., Bacci, T., Paoli, F., Viani, A., Vigliaturo, R., 2018. Assessment of the potential hazard represented by natural raw materials containing mineral fibres—The case of the feldspar from Orani, Sardinia (Italy). J. Hazard. Mater. 350, 76–87. https://doi.org/10.1016/j.jhazmat.2018.02.012

Gualtieri, A.F., Gatta, G.D., Arletti, R., Artioli, G., Ballirano, P., Cruciani, G., Guagliardi, A., Malferrari, D., Masciocchi, N., Scardi, P., 2019. Quantitative phase analysis using the Rietveld method: Towards a procedure for checking the reliability and quality of the results. Period. Mineral. 88, 147–151. https://doi.org/10.2451/2019PM870

IARC, 2012. Asbestos (chrysotile, amosite, crocidolite, tremolite, actinolite, and anthophyllite, in: IARC Monogr. Eval. Carcinog. Risks. Hum. IARC - International Agency for Research on Cancer, pp. 219–309.

Joshi, T.K., Bhuva, U.B., Katoch, P., 2006. Asbestos Ban in India: Challenges Ahead. Ann. N. Y. Acad. Sci. 1076, 292–308. https://doi.org/10.1196/annals.1371.072

Khorami, J., Choquette, D., Kimmerle, F.M., Gallagher, P.K., 1984. Interpretation of EGA and DTG analyses of chrysotile asbestos. Thermochim. Acta 76, 87–96. https://doi.org/10.1016/0040-6031(84)87006-9

Kolb, U., Mugnaioli, E., Gorelik, T.E., 2011. Automated electron diffraction tomography - a new tool for nano crystal structure analysis. Cryst. Res. Technol. 46, 542–554. https://doi.org/10.1002/crat.201100036

Larson, A.C., Von Dreele, R.B., 1994. General Structure Analysis System (GSAS). Los Alamos National Laboratory, Report LAUR 86-748.

Larson, T.C., Meyer, C.A., Kapil, V., Gurney, J.W., Tarver, R.D., Black, C.B., Lockey, J.E., 2010. Workers with Libby amphibole exposure: retrospective identification and progression of radiographic changes. Radiology 255, 924–933. https://doi.org/10.1148/radiol.10091447

Lemen, R., Landrigan, P., 2017. Toward an Asbestos Ban in the United States. Int. J. Environ. Res. Public. Health 14, 1302. https://doi.org/10.3390/ijerph14111302

Lin, R.-T., Chien, L.-C., Jimba, M., Furuya, S., Takahashi, K., 2019. Implementation of national policies for a total asbestos ban: a global comparison. Lancet Planet. Health 3, e341–e348. https://doi.org/10.1016/S2542-5196(19)30109-3

Lister, J., Bailey, S., 1967. Chlorite polytypism: IV. Regular two-layer structures. Am. Mineral. 52, 1614–1631.

Malferrari, D., Di Giuseppe, D., Scognamiglio, V., Gualtieri, A., 2021. Commercial brucite, a worldwide used raw material deemed safe, can be contaminated by asbestos. Period. Mineral. Vol. 90 No. 3 (2021). https://doi.org/10.13133/2239-1002/17384

Manceau, A., Chateigner, D., Gates, W.P., 1998. Polarized EXAFS, distance-valence least-squares modeling (DVLS), and quantitative texture analysis approaches to the structural refinement of Garfield nontronite. Phys. Chem. Miner. 25, 347–365. https://doi.org/10.1007/s002690050125

Marsili, D., Angelini, A., Bruno, C., Corfiati, M., Marinaccio, A., Silvestri, S., Zona, A., Comba, P., 2017. Asbestos Ban in Italy: A Major Milestone, Not the Final Cut. Int. J. Environ. Res. Public. Health 14, 1379. https://doi.org/10.3390/ijerph14111379

Mellini, M., 1982. The crystal structure of lizardite 1 T: hydrogen bonds and polytypism. Am. Mineral. 67, 587–598.

Ondrus, P., Veselovsky, F., Gabasova, A., Hlousek, J., Srein, V., Vavrin, I., Skala, R., Sejkora, J., Drabek, M., 2003. Primary minerals of the Jachymov ore district. J. Geosci. 48, 19–147.

Petriglieri, J.R., Salvioli-Mariani, E., Mantovani, L., Tribaudino, M., Lottici, P.P., Laporte-Magoni, C., Bersani, D., 2015. Micro-Raman mapping of the polymorphs of serpentine: Micro-Raman mapping of the polymorphs of serpentine. J. Raman Spectrosc. 46, 953–958. https://doi.org/10.1002/jrs.4695

Pohl, W., 1990. Genesis of magnesite deposits — models and trends. Geol. Rundsch. 79, 291–299. https://doi.org/10.1007/BF01830626

Rietveld, H., 1969. A profile refinement method for nuclear and magnetic structures. J. Appl. Crystallogr. 2, 65–71.

Schlossman, M., 2009. Chemistry and Manufacture of Cosmetics Volume 2: Formulating, 4th ed. Schlossman M.L., Allured Publishing Corporation.

Stanton, M.F., Layard, M., Tegeris, A., Miller, E., May, M., Morgan, E., Smith, A., 1981. Relation of particle dimension to carcinogenicity in amphibole asbestoses and other fibrous minerals. J. Natl. Cancer Inst. 67, 965–975.

Stanton, M.F., Wrench, C., 1972. Mechanisms of mesothelioma induction with asbestos and fibrous glass. J. Natl. Cancer Inst. 48, 797–821.

Steinfink, H., Sans, F., 1959. Refinement of the crystal structure of dolomite. Am. Mineral. 44, 679–681.

Terracini, B., 2019. Contextualising the policy decision to ban asbestos. Lancet Planet. Health 3, e331–e332. https://doi.org/10.1016/S2542-5196(19)30134-2

Thives, L.P., Ghisi, E., Thives Júnior, J.J., Vieira, A.S., 2022. Is asbestos still a problem in the world? A current review. J. Environ. Manage. 319, 115716. https://doi.org/10.1016/j.jenvman.2022.115716

Toby, B.H., 2001. EXPGUI, a graphical user interface for GSAS. J. Appl. Crystallogr. 34, 210–213. https://doi.org/10.1107/S0021889801002242

Tzamos, E., Bussolesi, M., Grieco, G., Marescotti, P., Crispini, L., Kasinos, A., Storni, N., Simeonidis, K., Zouboulis, A., 2020. Mineralogy and Geochemistry of Ultramafic Rocks from Rachoni Magnesite Mine, Gerakini (Chalkidiki, Northern Greece). Minerals 10, 934. https://doi.org/10.3390/min10110934

Van Gossen, B., Lowers, H., Sutley, S., Gent, C., Castor, S., Papke, K., Meeuwig, R., 2003. Asbestos-bearing talc deposits, southern Death Valley region, California, in: Proceedings of the 39th Forum on the Geology of Industrial Minerals. Presented at the Betting on industrial minerals, Reno/Sparks, Nevada, pp. 215–223.

Worliczek, E., 2017. Naturally Occurring Asbestos: The Perception of Rocks in the Mountains of New Caledonia, in: Dürr, E., Pascht, A. (Eds.), Environmental Transformations and Cultural Responses. Palgrave Macmillan US, New York, pp. 187–214. https://doi.org/10.1057/978-1-137-53349-4_8

Yoon, Y.-R., Kwak, K., Choi, Y., Youn, K., Bahk, J., Kang, D.-M., Paek, D., 2018. The Asbestos Ban in Korea from a Grassroots Perspective: Why Did It Occur? Int. J. Environ. Res. Public. Health 15, 198. https://doi.org/10.3390/ijerph15020198

Figure captions

Fig 1. Graphical output of the Rietveld refinement of KT1 (a) and KG1 (b) powder samples. Red crosses represent the observed pattern, the thin green line represents the calculated pattern, and the blue bottom line is the difference line. The vertical bars mark of the peaks of each crystalline phase included in the refinement procedure which are (from the bottom): magnesite, dolomite, serpentine and quartz (a); magnesite, dolomite, serpentine, quartz, talc, chlorite, calcite and smectite (b).

Fig. 2. Thermal behaviour of samples KT1. (a) TGA (solid lines) and DTG (dashed lines) curves; (b) DTA curve (the maxima denote exothermic reactions); (c) MSEGA curves for H_2O (m/z=18) and CO_2 (m/z=44); the curves for NO (m/z=30) and SO_2 (m/z=64) are not reported as these gasses were not detected.

Fig. 3. Macroscopic (a) and microscopic (b) observation of KT2 sample. (a) KT2 sample occurs as centimetric fragments of grey-white rock with green veins (I); a magnification of the area marked by the white arrow in (I) shows that the green veins are characterised by an intergrowth of green plate-like mineral grains with white mineral fibre bundles highlighted by the white arrows (II). (b) Chrysotile fibres observed with PCOM in bright (I) and (II) and dark (III) and (IV) field. Fibres perpendicular to the polarizer, in bright field, have pale blue colour and orange halo (I); fibres parallel to the polarizer, in bright field, have dark blue colour and orange halo (II); fibres perpendicular to the polarizer, in dark field, have blue colour (III); fibres parallel to the polarizer, in dark field, have purple colour (IV). The images (III) and (IV)

show the Walton-Beckett graticule (100 µm in diameter) to identify the length and width of the fibres.

Fig. 4. Representative SEM images of Turkish and Greek magnesite samples: (a) flexible chrysotile bundle with frayed and split ends dipped in a matrix of massive magnesite particles in sample KT1; (b) detail of chrysotile fibres in magnesite fragments presents in sample KG1; (c) elongated fibrous bundle with split ends in sample KT2; (d) detail of chrysotile fibres dipped in a matrix massive magnesite particle in sample KG2; (e-f) representative EDX spectra of the chrysotile fibres and magnesite particles shown in (a) and (b), rispectively.

Fig. 5. Representative TEM images of the magnesite samples KT2 (a-e) and KG2 (f). (a) High-angle annular dark-field images of chrysotile fibres; (b) A chrysotile fibre with a particularly large channel of about 40 nm in diameter; (c) Massive fragments with composition, consistent with serpentine minerals; (d) Reconstructed 3DED volume showing typical crowns of diffuse scattering produced by the bending of the serpentine layers to form chrysotile; (e) Reconstructed 3DED data set from a massive polygonal serpentine; (f) Examples of bent hair-like fibres typically arranged in bundles.

Fig. 6. Raman spectra of KT1, KG1 and KT2 in the low-wavenumber (a) and in the OH-stretching (b) spectral regions.

Table 1.

Qualitative phase analysis of the samples KT1, KG1, KT2, KG2, and VA.

Sample	Mineral phases
KT1	magnesite, dolomite, serpentine, quartz
KG1	magnesite, dolomite, smectite, quartz, serpentine, calcite, chlorite, talc
KT2	magnesite, dolomite, serpentine, quartz
KG2	magnesite, dolomite, serpentine
VA	magnesite

Table 2.

Mineralogical composition of KT1 and KG1 powder samples (wt%) obtained from the Rietveld quantitative phase analysis. The standard deviation σ_Q (values in parenthesis) of the weight percentage Q of each phase was also calculated in the GSAS software (Larson and Von Dreele, 1994).

Sample	**KT1**	**KG1**
R_{wp} (%)	13.4	14.8
R_p (%)	10	11.0
χ^2	7.5	9.3
magnesite	92.81(3)	92.43(3)
dolomite	4.7(1)	2.2(1)
quartz	0.67(4)	1.4(1)
talc	-	0.1(1)
chlorite	-	0.3(2)
calcite	-	0.5(1)
smectite	-	2.2(2)
serpentine	**1.8(1)**	**0.8(2)**

Figure 1

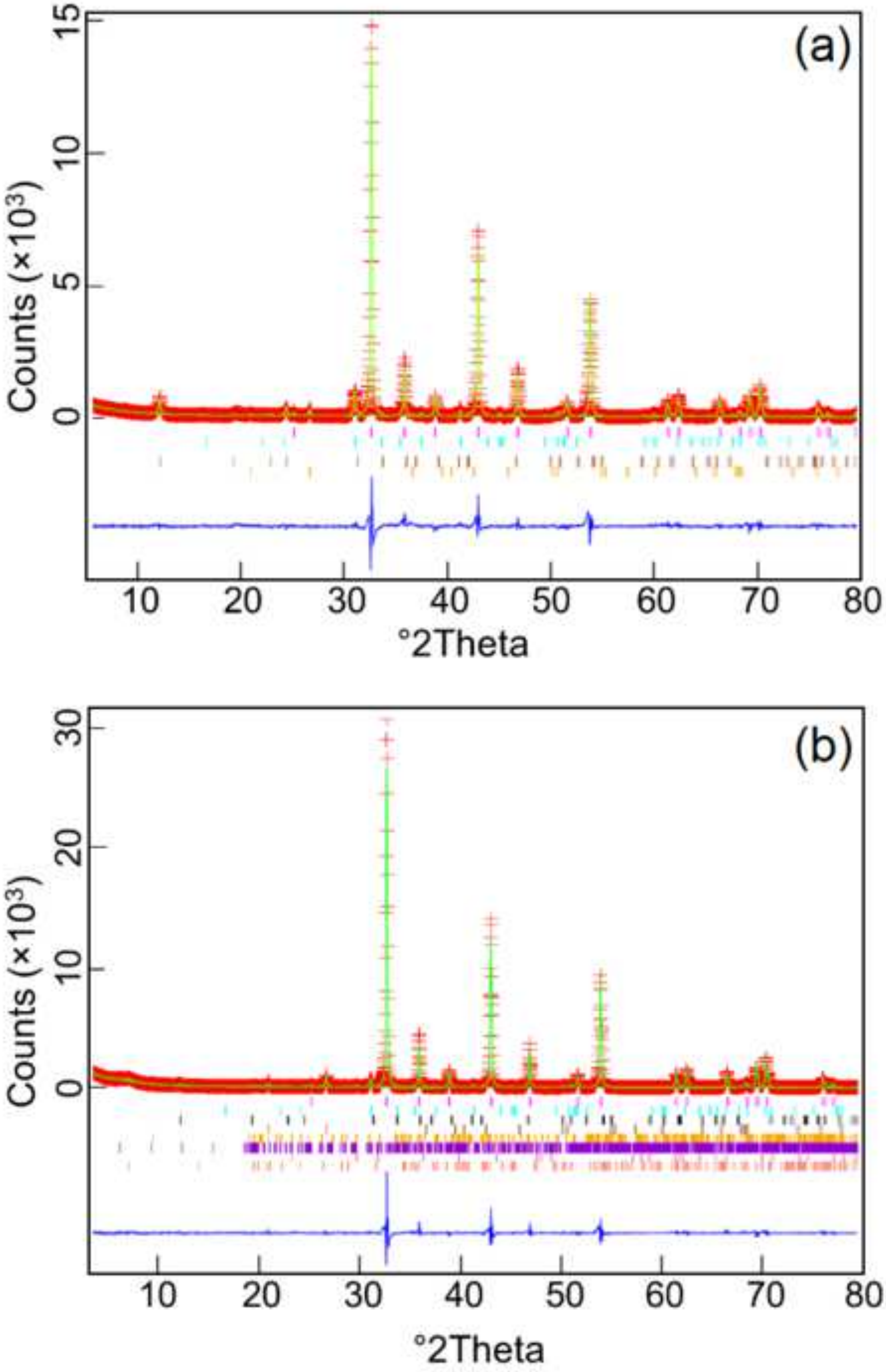
(a)
Counts (×10³)
0
5
10
15
10
20
30
40
50
60
70
80
°2Theta
(b)
Counts (×10³)
0
10
20
30
10
20
30
40
50
60
70
80
°2Theta

Figure 2

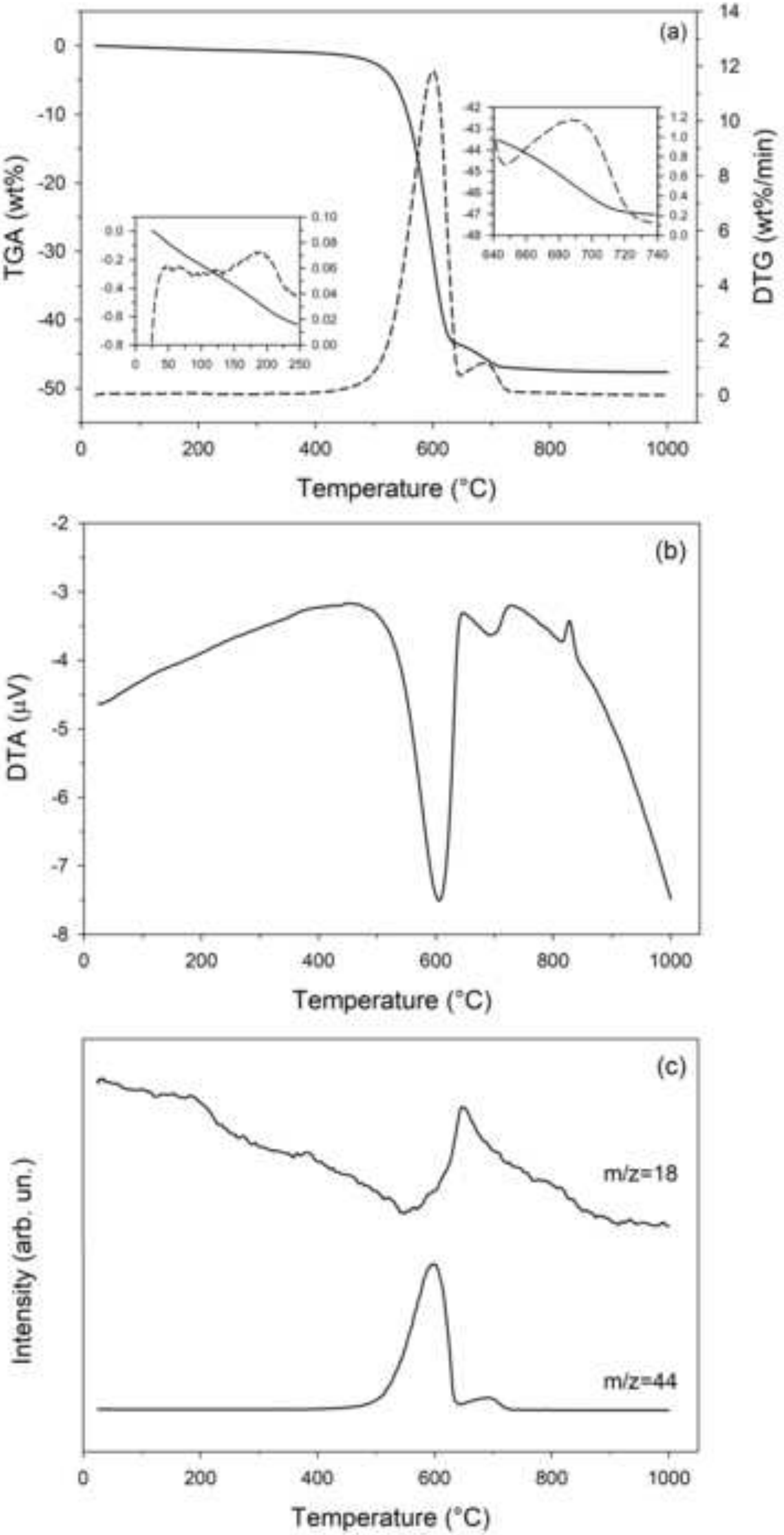
(a)
TGA (wt%)
DTG (wt%/min)
0
-10
-20
-30
-40
-50
14
12
10
8
6
4
2
0
0.0
-0.2
-0.4
-0.6
-0.8
0.10
0.08
0.06
0.04
0.02
0.00
0
50
100
150
200
250
-42
-43
-44
-45
-46
-47
-48
1.2
1.0
0.8
0.6
0.4
0.2
0.0
640
660
680
700
720
740
0
200
400
600
800
1000
Temperature (°C)
(b)
DTA (µV)
-2
-3
-4
-5
-6
-7
-8
0
200
400
600
800
1000
Temperature (°C)
(c)
Intensity (arb. un.)
m/z=18
m/z=44
0
200
400
600
800
1000
Temperature (°C)

Figure 3

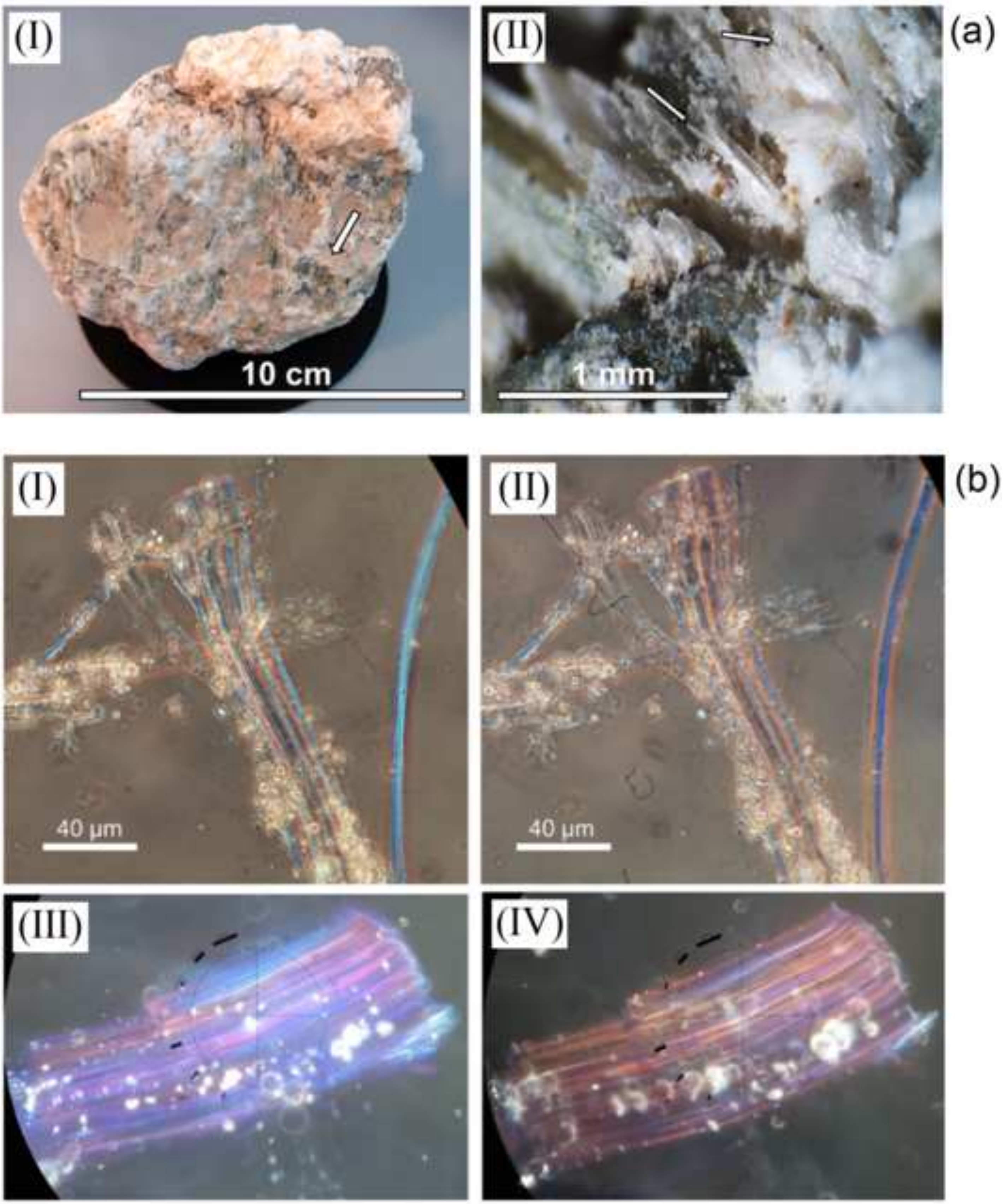

Figure 4

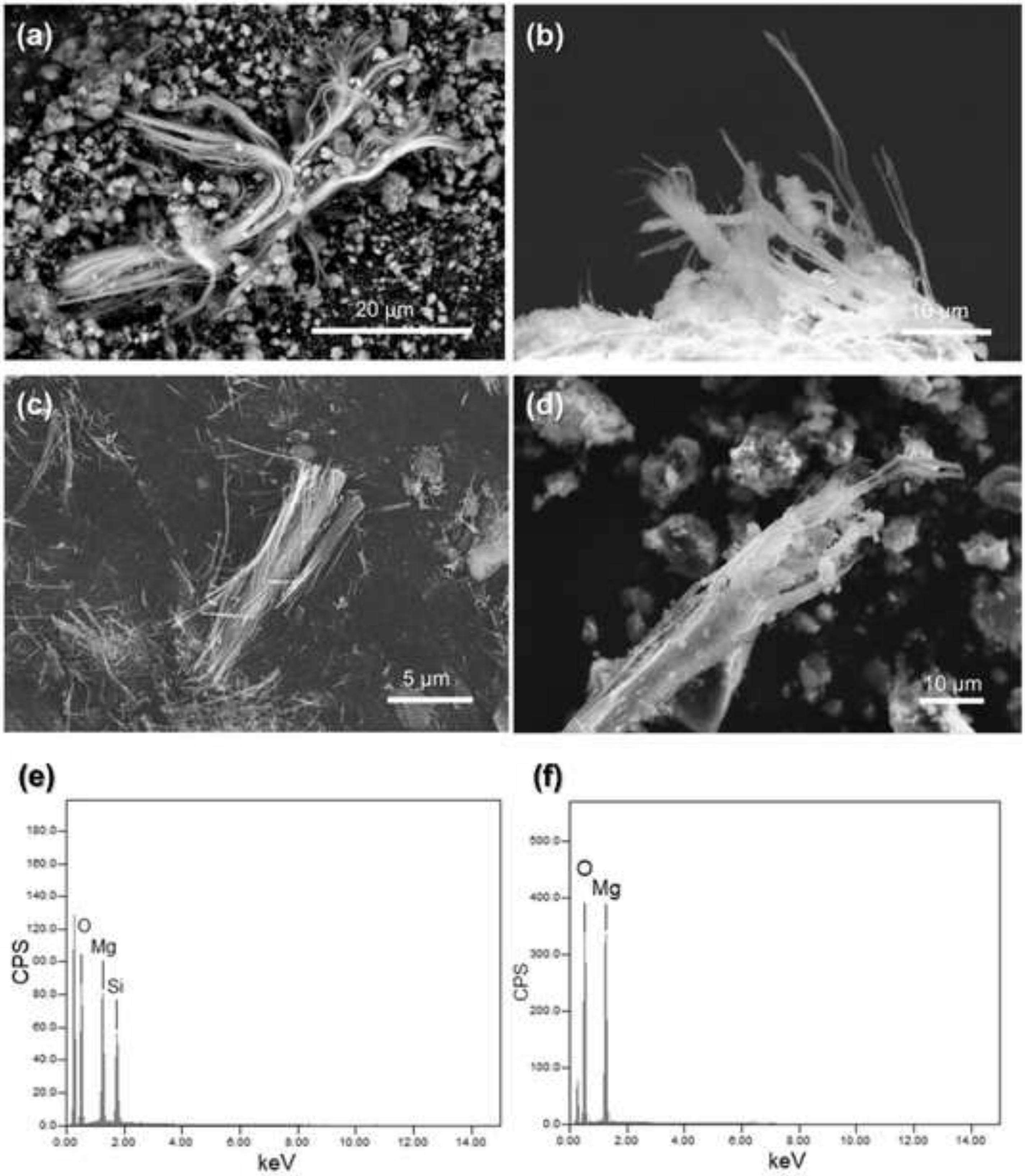
(a)
20 µm
(b)
10 µm
(c)
5 µm
(d)
10 µm
(e)
CPS
180.0
160.0
140.0
120.0
100.0
80.0
60.0
40.0
20.0
0.0
O
Mg
Si
0.00
2.00
4.00
6.00
8.00
10.00
12.00
14.00
keV
(f)
CPS
500.0
400.0
300.0
200.0
100.0
0.0
O
Mg
0.00
2.00
4.00
6.00
8.00
10.00
12.00
14.00
keV

Figure 5

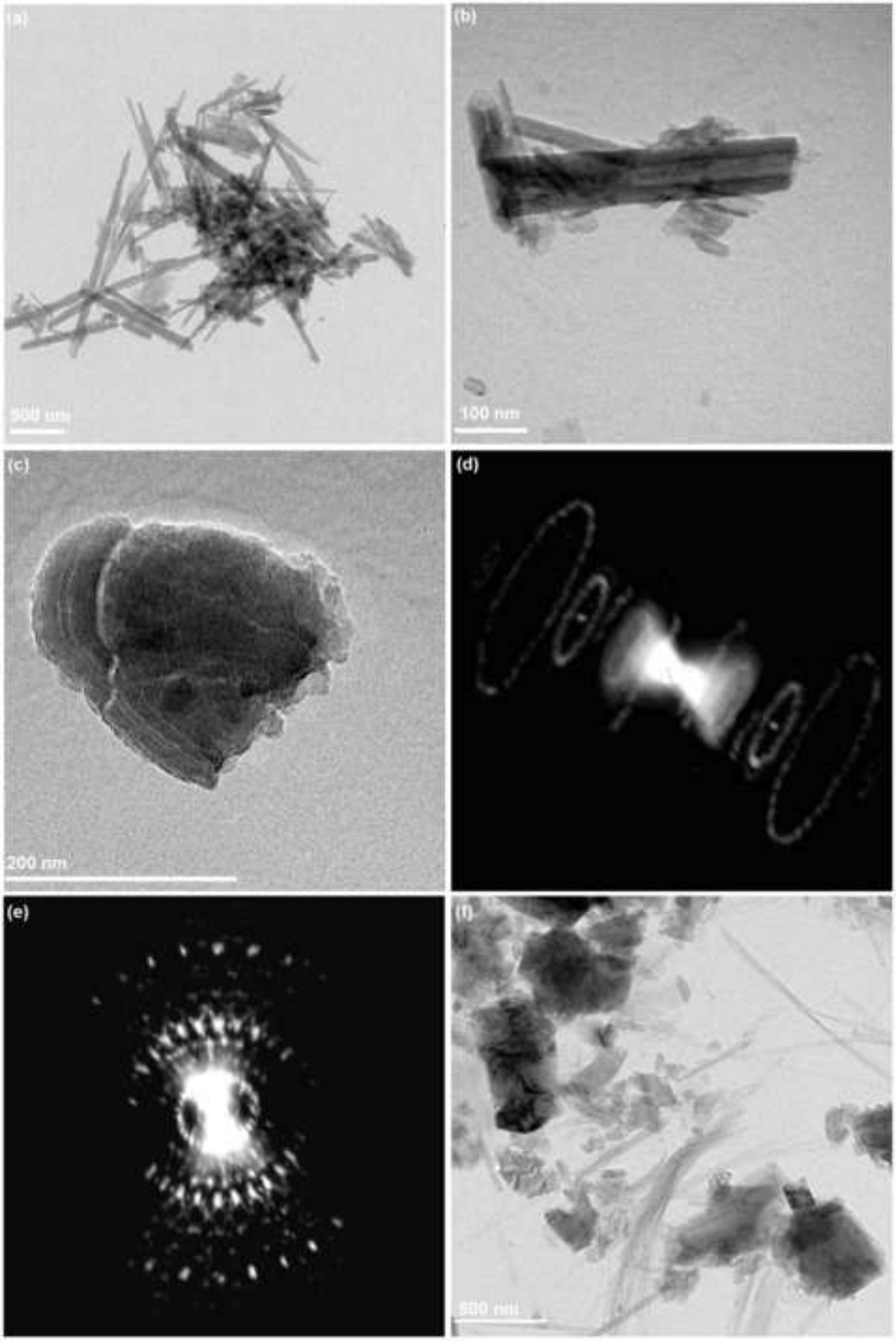

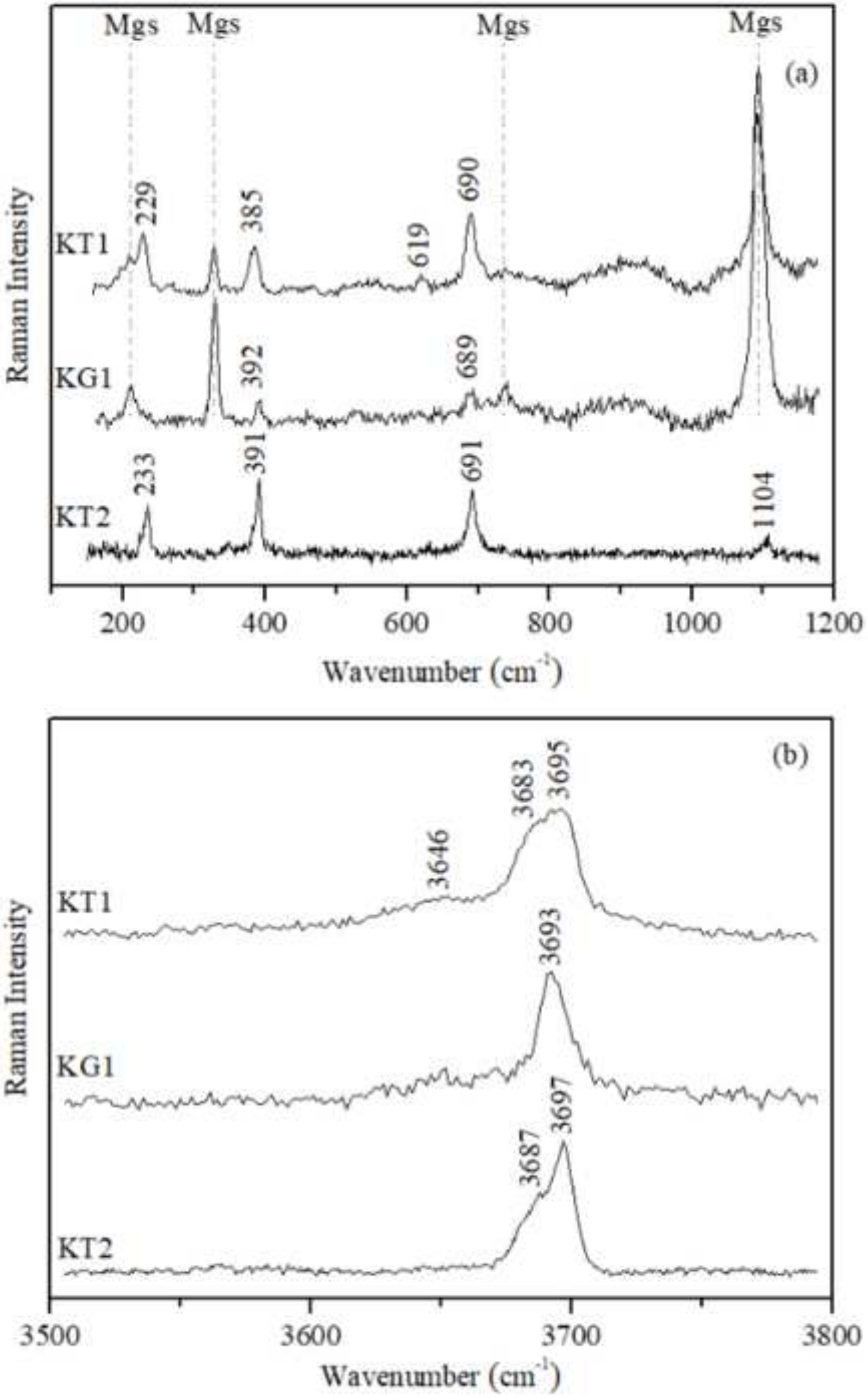
Mgs
Mgs
Mgs
Mgs
(a)
Raman Intensity
KT1
229
385
619
690
KG1
392
689
KT2
233
391
691
1104
200
400
600
800
1000
1200
Wavenumber (cm-1)
(b)
Raman Intensity
KT1
3646
3683
3695
KG1
3693
KT2
3687
3697
3500
3600
3700
3800
Wavenumber (cm-1)